ACS OMEGA

Article

http://pubs.acs.org/journal/acsodf

Essential Dynamics of an Effective Phototherapeutic Drug in a Nanoscopic Delivery Vehicle: Psoralen in Ethosomes for Biofilm Treatment

Damayanti Bagchi,[†] Shreyasi Dutta,[†] Priya Singh, Siddhi Chaudhuri, and Samir Kumar Pal*

Department of Chemical, Biological and Macromolecular Sciences, S. N. Bose National Centre for Basic Sciences, Block JD, Sector III, Salt Lake, Kolkata 700 106, India

ABSTRACT: Appropriate localization of a drug and its structure/functional integrity in a delivery agent essentially dictates the efficacy of the vehicle and the medicinal activity of the drug. In the case of a phototherapeutic drug, its photoinduced dynamics becomes an added parameter. Here, we have explored the photoinduced dynamical events of a model phototherapeutic drug psoralen (PSO) in a potential delivery vehicle called an ethosome. Dynamic light scattering confirms the structural integrity of the ethosome vehicle after the encapsulation of PSO. Steady state and picosecond resolved polarization gated spectroscopy, including the well-known strategy of solvation and Förster resonance energy transfer, reveal the localization of the drug in the vehicle and the environment in the proximity of PSO. We have also investigated the efficacy of drug delivery to various individual bacteria (Gram-negative: *Escherichia coli*; Gram-positive: *Staphylococcus aureus*) and bacterial biofilms. Our optical and electron microscopic studies reveal a significant reduction in bacterial survival (∼70%) and the destruction of bacterial adherence following a change in the morphology of the biofilms after phototherapy. Our studies are expected to find relevance in the formulation of drug delivery agents in several skin diseases and biofilm formation in artificial implants.

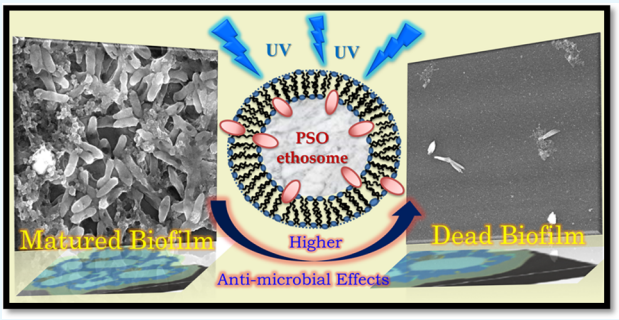

INTRODUCTION

Over the past 2 decades, photodynamic therapy has been harnessed for the treatment of a broad range of diseases.[1,2] The action of this therapy is based on the topical application of a photosensitive drug (photosensitizer) followed by irradiation, usually in the ultraviolet-A (UVA: 320−400 nm) or visible (vis: 400−720 nm) region of the spectrum.[3,4] The photosensitizer will absorb the radiation and conduct the excitation energy into the tissue. This phenomenon leads to an array of photochemical redox and/or radical reactions.[5] The family of linear furocoumarins and their derivatives, more customarily known as psoralen (PSO), have been shown to be active dermal photosensitizing agents in the presence of UVA.[6−8] PSO intercalates with DNA upon irradiation with UVA and subsequently forms adducts with pyrimidine bases in the opposite strand of DNA, resulting in DNA strand cross-linking.[9,10] These result in the inhibition of cell division; thus, PSO followed by UV radiation is widely used for the treatment of psoriasis.[11,12]

The efficacy of a drug depends on its penetration capability within the phospholipid membrane of the cell, which is necessary for it to reach its cellular targets.[13] The major difficulty with naturally occurring PSO is its insolubility in water, which leads to weak percutaneous permeability and poor deposition in the skin.[14,15] The poor solubility of the drug usually requires that it is frequently administered, increasing the risk of adverse reactions.[15] Topical delivery of drugs by liposomal formulations has attracted considerable interest in recent decades because of the improved therapeutic effects.[16,17] However, classical liposomes are of little use because they cannot penetrate the cellular or bacterial membrane.[18] On the other hand, several lines of research have indicated that ethosomes, which are in a class of liposomes containing some amount of ethanol in the core, could be a better tool for the subdermal delivery of macromolecules.[19,20] Earlier, it was shown that as the concentration of ethanol in ethosomes increases from 20 to 45%, the drug entrapment efficiency improves owing to an elevation in the fluidity of the membrane.[21] Several in vitro and in vivo studies have demonstrated the enhanced skin permeation and bioavailability of different therapeutic agents from a biocompatible ethosomal formulation.[22,23] For instance, Dubey et al. prepared an ethosomal formulation of indinavir, an anti-HIV drug, and investigated its augmented transdermal delivery potential.[24] Our previous articles reported the delivery of significant photosensitizers using zinc oxide nanoparticles (ZnO NPs) as a competent drug delivery vehicle, where an increased efficacy

Received: February 17, 2017
Accepted: April 28, 2017
Published: May 5, 2017

DOI: 10.1021/acsomega.7b00187
ACS Omega 2017, 2, 1850−1857

of the phototherapeutic drugs upon conjugation with ZnO NPs was also successfully observed.[25−27]

Although research studies have reported the topical delivery of PSO via ethosomes,[28] very little is known about the photoinduced dynamics of PSO encapsulated in this drug delivery vehicle. In the present study, we synthesized ethosomes of 110 nm vesicular size and entrapped PSO in the ethosomal formulation (PSO−ethosome), which was characterized by UV−vis absorption and steady state fluorescence spectroscopic methods and dynamic light scattering (DLS) studies. A well-known solvation probe, 4-(dicyanomethylene)-2-methyl-6-(*p*-dimethylaminostyryl)-4*H*-pyran (DCM),[29] was employed to study solvent relaxation in the ethosomes.[30] Picosecond-resolved Förster resonance energy transfer (FRET) was exploited to confirm the colocalization of PSO in ethosomes with crystal violet (CV), a well-known ethosome-binding organic dye.[31] After thorough characterization of the interfacial events, the PSO−ethosomes were evaluated for their photoinduced antibacterial activity toward Gram-negative *Escherichia coli* and Gram-positive *Staphylococcus aureus*.

Life-threatening bacterial diseases originate due to the formation of biofilms, making bacterial infections challenging to cure. The extracellular polymeric substances (EPS) comprising the biofilm prevent the penetration of drugs into the biofilm.[32,33] Thus, we employed PSO−ethosomes to study the eradication of biofilms because this requires the efficient penetration and accumulation of the drug into the biofilm network. A CV assay was used to assess the antibiofilm activity of PSO−ethosomes against *E. coli* and *S. aureus*.[34] We further performed scanning electron microscopy to observe the morphological changes of the biofilm upon treatment with PSO−ethosomes in the presence of UVA. Therefore, our studies investigate a permeation-enhancing carrier, ethosomes, which facilitate the transport of PSO through a biological barrier: the bacterial membrane or cell wall. This may result in an alternative use and an enhanced efficiency of ethosomes as a drug delivery vehicle for antibiotic-resistant biofilms.

RESULTS AND DISCUSSION

Ethosomes are a soft vesicle composed of phospholipids (PC), a high concentration of ethanol, and water. In our study, we synthesized ethosomal solutions having characteristic spherical droplets with an average hydrodynamic diameter of 110 nm measured by DLS (inset of Figure 1a). Absorption spectra of PSO in a water−ethanol mixture and in ethosomes are shown in Figure 1a, which shows that PSO in a water−ethanol mixture (red) has three peaks at 244, 294, and 340 nm. PSO encapsulated in ethosomes (blue) also shows three peaks with an uplifted baseline due to scattering of colloidal ethosomes. The transitions at 294 and 340 nm are reported to result from the n → π^* transition of nonbonding electrons on the C-2 carbonyl group in PSO and the $\pi \rightarrow \pi^*$ transition of π electrons of the PSO ring system, respectively.[7] We estimated that 88.7 μM PSO is associated with 3.4 μM ethosomes. In other words, 26 PSO molecules are attached to each ethosome vesicle. Emission spectra of PSO in a water−ethanol mixture (red) and PSO−ethosomes (blue) (Figure 1b) show that the fluorescence intensity of PSO is quenched upon its encapsulation in ethosomes. The quenching of the emission of PSO in a nonpolar medium, cyclohexane (green), is also shown in Figure 1b. The quantum yield of PSO in aqueous ethanol, ethosomes, and cyclohexane are estimated to be 1.0 × 10^{-2}, 6.0 × 10^{-3}, and 2.0 × 10^{-4}, respectively, consistent with the literature.[35] Studies on the spectroscopic properties of PSO have reported that the lowest excited state (singlet and triplet) energies of PSO are strongly dependent on the polarity of the solvent. As the polarity of the solvent increases, the energy level ordering of PSO is assumed to change and thereby fluorescence becomes predominant compared to nonradiative intersystem crossing.[35,36] Upon encapsulation into ethosomes, the polarity of the solvent around PSO decreases, which results in a quenching of the fluorescence intensity without changing the emission maxima. The similarity of the quantum yield of PSO in ethosomes with polar aqueous ethanol indicates that the location of the probe is at the interface. We have also recorded excitation spectra (Figure 1b, inset) of PSO in water−ethanol and PSO−ethosomes, which are similar to the corresponding absorption spectra. Figure 1c shows picosecond resolved

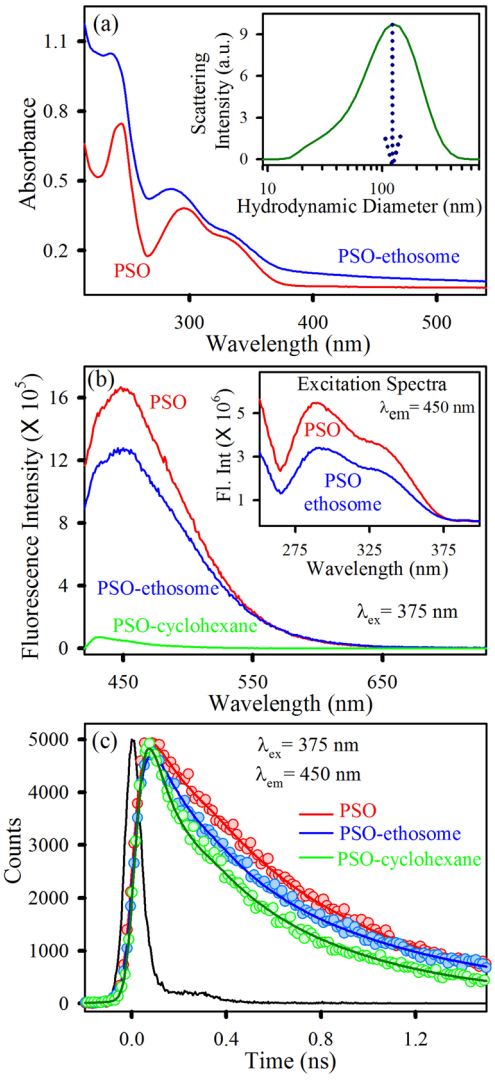

Figure 1. (a) UV−vis absorption spectra of PSO in water−ethanol mixture (red) and PSO−ethosomes (blue). The inset shows the hydrodynamic diameter of the ethosomes measured by DLS. (b) Room-temperature emission spectra of PSO (red), PSO−ethosomes (blue), and PSO in cyclohexane (green). The excitation wavelength is 375 nm. The inset shows the excitation spectra of PSO (red) and PSO−ethosome (blue). (c) Fluorescence transients of PSO in water−ethanol mixture (red), PSO−ethosomes (blue), and PSO in cyclohexane (green).

DOI: 10.1021/acsomega.7b00187
ACS Omega 2017, 2, 1850−1857

emission transients of PSO in various media including ethosomes. The numerical fitting of the transients reveals an average time constant of 0.62 ns for aqueous ethanol and 0.34 ns for cyclohexane. In ethosomes, the average time constant of 0.50 ns is close to that in aqueous ethanol, revealing that the location of PSO is at the interface.

To compare the microenvironment of the ethosomes with liposomes, we used a well-known fluorescent solvation probe, DCM, which is widely used in the characterization of various liposomes.[37,38] The inset of Figure 2a represents the excitation and emission spectra of DCM in ethosomes. The emission peak of DCM in ethosomes is blue-shifted to 570 nm compared to that of DCM in buffer. This corresponds to the binding of DCM to the hydrophobic core of the ethosomes. Figure 2a shows fluorescence transients of DCM encapsulated in the ethosomes at three characteristic detection wavelengths (510, 580, and 670 nm), which fall in the blue, peak, and red end of the emission spectrum of the probe in the ethosomes. In the excited state of DCM, intramolecular charge transfer takes place, which gives rise to a very high dipole moment (23.6 D) compared to the ground state.[39] In the blue edge of the spectrum (510 nm), the observation is consistent with the fact that DCM undergoes solvation relaxation, where the signal is seen to decay faster compared to the red edge (670 nm), whereas a rise component is apparent in ethosomes. Using the fitting parameters of the fluorescence decay and the steady state emission spectrum, the time-resolved emission spectra (TRES) and the solvent correlation function ($C(t)$) of DCM in ethosomes were constructed (Figure 2b,c). The associated dynamical Stokes shift ($\Delta\nu$) of DCM in ethosomes is calculated to be 1458 cm^{-1}. It is evident that due to the finite time resolution of our instrument (20−30 ps), we missed some portion of the dynamics. We calculated the missing component to be ∼17% following the procedure of Fee and Maroncelli.[40,41] The $C(t)$ decay of DCM is fitted with a biexponential function with two time components of 430 ps (44%) and 3.04 ns (56%). The time constants are consistent with the reported values of the solvation relaxation time of DCM in dipalmitoylphosphatidylcholine (DPPC) liposomes.[38] The temporal decay of fluorescence anisotropy $r(t)$ of DCM in ethosomes is shown in the inset of Figure 2c. The decay transient can be fitted monoexponentially with a time constant of 38 ps (29%), with a significant part (71%) that persists within our experimental time window of 20 ns (we show up to 4 ns). The faster time constant is consistent with the tumbling motion of DCM in the ethosomes.[38]

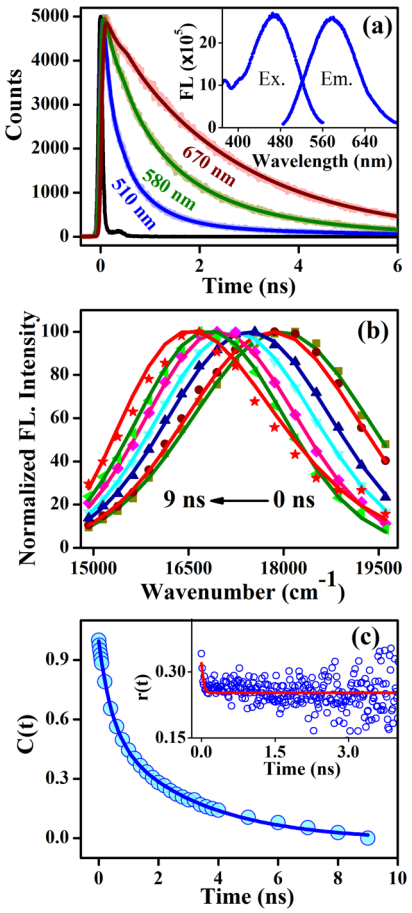

Figure 2. (a) Fluorescence transients at different wavelengths for DCM−ethosomes. The inset shows excitation and emission spectra of DCM. (b) TRES. (c) Decay of the solvation correlation function, $C(t)$, with time. The inset shows temporal decay of fluorescence anisotropy, $r(t)$, of DCM−ethosomes.

To study the colocalization of a model cationic drug with hydrophobic DCM in ethosomes, we used CV and employed a FRET strategy. Figure 3a shows the spectral overlap of energy donor DCM emission with the absorption spectrum of acceptor CV. A significant quenching of the steady-state emission of DCM in the presence of CV in ethosomes is observed, where the DCM:CV concentration in the ethosomal mixture is 1:1 (inset of Figure 3b). The picosecond-resolved fluorescence decay profile of DCM in the absence (green) and presence (blue) of CV was monitored at 620 nm upon excitation at 375 nm (Figure 3b). The shorter component in the decay profile suggests an excited state energy transfer process (Table 1). A FRET efficiency of ∼75% with an average donor−acceptor distance of 5.8 nm was calculated for the DCM−CV pair (Table 1). It is also observed that the distance between DCM and CV is independent of the detection wavelength by detecting fluorescence transients at different wavelengths (data not shown). This indicates that DCM is homogeneously distributed in the ethosomal mixture. It is reported that the maximum thickness of a phospholipid bilayer is 7.3 nm.[42] Therefore, the possible location of CV could be at the polar interface of the ethosome.

After having an idea about the location of CV with respect to DCM, we exploited the spectral overlap of CV with PSO to study the localization of PSO in the ethosomes. A considerable spectral overlap of PSO's emission with the absorption spectrum of CV is shown in Figure 3c, where the concentration of PSO:CV is 1:10, indicating the possibility of FRET from PSO to CV in the ethosome. A significant quenching of the steady state emission of PSO in the presence of CV in the ethosome is observed (inset of Figure 3d). The picosecond-resolved fluorescence decay profile of PSO in ethosomes in the absence (red) and presence (cyan) of CV was monitored at 450 nm upon excitation at 375 nm (Figure 3d). The excited state lifetime (τ_{av}) of PSO is reduced upon interaction with CV. Details of the fitting parameters for the fluorescence decay are provided in Table 1. We estimated the FRET efficiency to be ∼84% and the donor (PSO)−acceptor (CV) distance to be ∼2.2 nm. This distance is almost independent of the detection wavelength because there is no indication of a change in the lifetime by changing the detection wavelength. More details are provided in Table 1. The comparatively shorter donor−

DOI: 10.1021/acsomega.7b00187
ACS Omega 2017, 2, 1850−1857

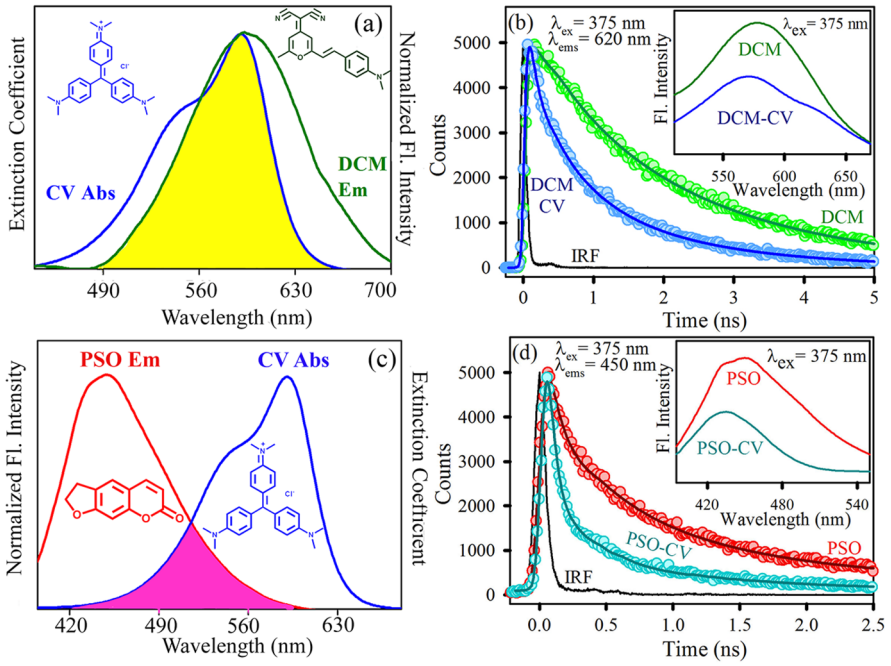

Figure 3. (a) Overlap of DCM−ethosome emission and CV absorption in water. (b) Picosecond-resolved fluorescence transients of DCM−ethosomes (excited at 375 nm) in the absence (green) and presence (blue) of CV collected at 620 nm. The inset shows steady state emission spectra of DCM−ethosomes in the absence (green) and presence (blue) of CV. (c) Overlap of PSO−ethosome emission and CV absorption in water. (d) Picosecond-resolved fluorescence transients of PSO−ethosome (excited at 375 nm) in the absence (red) and presence (cyan) of CV collected at 450 nm. The inset shows steady state emission spectra of PSO−ethosomes in the absence (red) and presence (cyan) of CV.

Table 1. Time-Resolved Fluorescence Decay (Excitation at 375 nm) and FRET Data of PSO and DCM in Ethosomes in the Absence and Presence of CV[a]

fluorescence transients					
wavelength (nm)	system	τ_1 (ns)	τ_2 (ns)	τ_3 (ns)	τ_{avg} (ns)
450	PSO	0.08 (51%)	0.58 (33%)	2.59 (16%)	0.65
	PSO−CV	0.03 (83%)	0.22 (12%)	1.10 (05%)	0.11
620	DCM		0.72 (23%)	2.34 (77%)	1.97
	DCM-CV	0.11 (36%)	0.61 (36%)	1.83 (28%)	0.77

FRET parameters						
wavelength (nm)	system	Q_D	$J(\lambda)$ (M^{-1} cm^{-1} nm^4)	E (%)	R_0 (nm)	R (nm)
450	PSO−CV	6.0×10^{-3}	4.35×10^{15}	85	3.33	2.19
620	DCM−CV	0.35	1.09×10^{16}	60	7.42	5.85

[a]Values in parentheses represent the relative weight percentage of the time component with a standard error of ca. 10%.

acceptor distance in the case of PSO−CV can be attributed to the higher concentration of CV in the present case compared to the former one.

Lastly, we evaluated PSO−ethosomes as an antimicrobial agent followed by a drug delivery system to inhibit the growth of bacterial biofilms. PSO−ethosomes were employed as a potential photodynamic agent to inhibit the growth of Gram-negative *E. coli* and Gram-positive *S. aureus*. For photodynamic therapy experiments, we added PSO−ethosomes (85 μM PSO) to bacterial cultures in the presence and absence of UVA. The inhibition of bacterial growth after photodynamic treatment is clearly visible. For comparison, the colonies were counted for control and PSO−ethosome-treated plates. The colony forming units (CFUs) indicate insignificant antibacterial activity of PSO−ethosomes in the dark. In the case of samples treated with PSO−ethosomes and UVA irradiation, the bacterial growth was inhibited sharply, indicating immense photo-induced antimicrobial activity of PSO−ethosomes. The maximum inhibition of *E. coli* was obtained for PSO−ethosome-treated samples, where a 95% decrease in CFUs was observed after photodynamic treatment (Figure 4a). Figure 4b,c clearly shows *E. coli* cultures treated with PSO−ethosomes in the absence and presence of UVA light. The inhibition of bacterial growth after photodynamic treatment is clearly visible. A similar trend was observed for Gram-positive bacteria *S. aureus* (Figure 5a), demonstrating the enormous photodynamic antibacterial activity of PSO−ethosomes. The pictures of *S. aureus* culture plates (Figure 5b,c) clearly show visual differences of PSO−ethosome-treated bacteria in the absence and presence of UVA. Control experiments using ethosomes without PSO show no significant antibacterial effect.

A biofilm is a microbial community that has a compact and complex structure and is often encapsulated within a matrix of polymeric material that consists of intricate networks of cells attached to abiotic surfaces.[43] Upon formation of a biofilm, microbes can resist antibiotics and immune cell challenge and

DOI: 10.1021/acsomega.7b00187
ACS Omega 2017, 2, 1850−1857

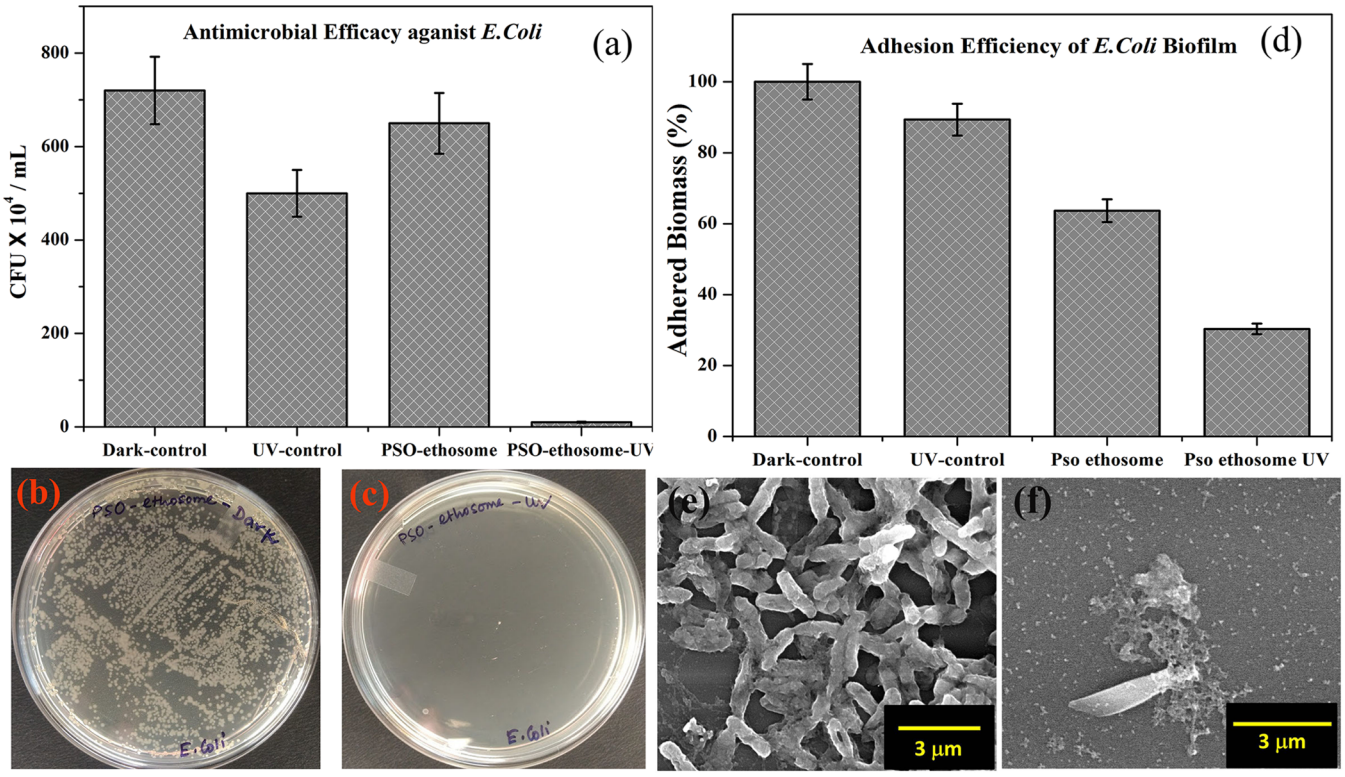

Figure 4. (a) Antibacterial activity of PSO−ethosomes against *E. coli* in the absence and presence of UVA. (b, c) Images of PSO−ethosome-treated *E. coli* culture plates before and after UVA irradiation, respectively. (d) Adhesion efficiency of PSO−ethosome-treated *E. coli* biofilms in the absence and presence UVA irradiation. SEM images of an *E. coli* biofilm (e) without treatment and (f) treated with PSO−ethosomes followed by UVA illumination for 30 min.

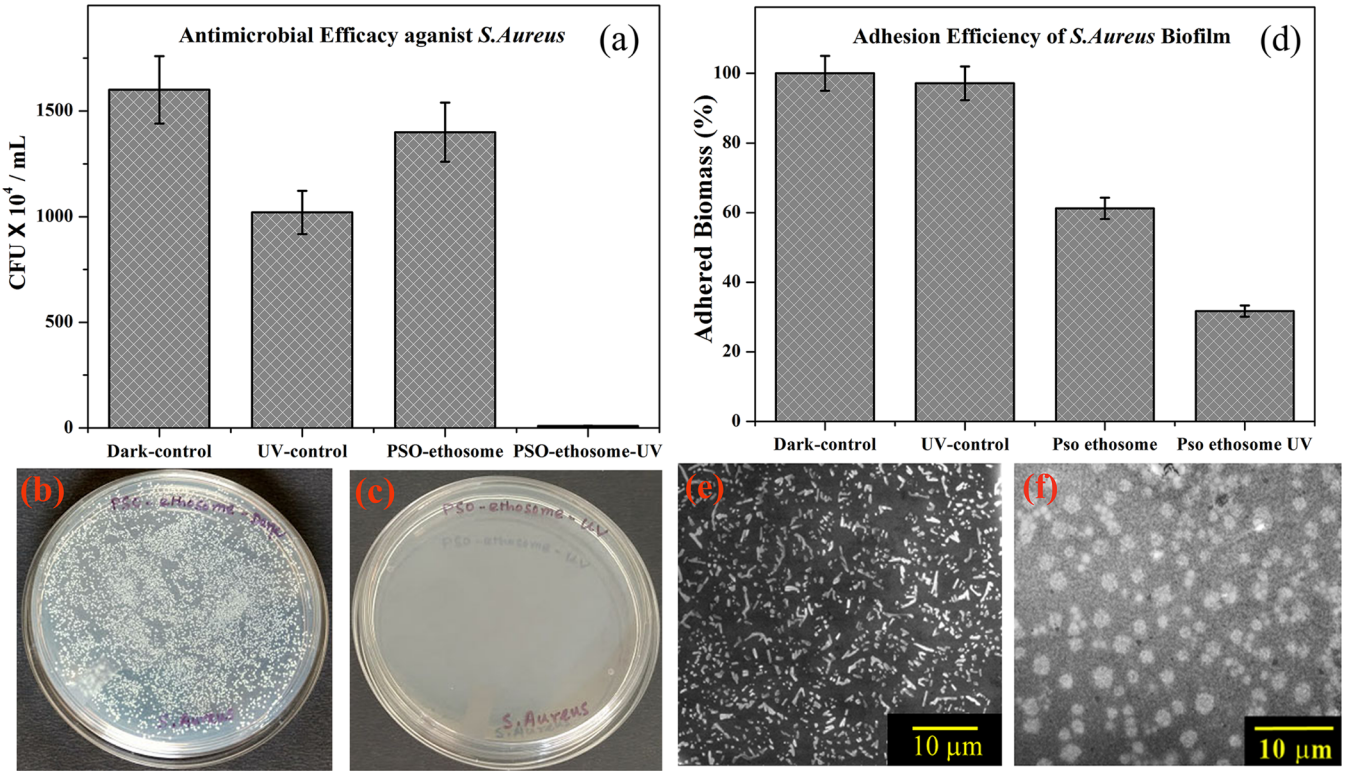

Figure 5. (a) Antibacterial activity of PSO−ethosomes against *S. aureus* in the absence and presence of UVA. (b, c) Images of PSO−ethosome-treated *S. aureus* culture plates before and after UVA irradiation, respectively. (d) Adhesion efficiency of PSO−ethosome-treated *S. aureus* biofilms in the absence and presence UVA irradiation. SEM images of an *S. aureus* biofilm (e) without treatment and (f) treated with PSO−ethosomes followed by UVA illumination for 30 min.

DOI: 10.1021/acsomega.7b00187
ACS Omega 2017, 2, 1850−1857

can be deeply inserted into the cracks and pores of solid surfaces and metallic and nonmetallic medical devices like catheters, implants, and dental materials.[44] For our study, biofilm formation by *E. coli* and *S. aureus* was measured after 48 h. The total adhered biomass of the biofilms was monitored through a quantitative assay using CV. There is a decrease in biomass (~30%) for both bacteria (*E. coli* and *S. aureus*) treated with ethosome-containing PSO. The bacterial biomass could be further reduced to ~60% when PSO−ethosome-treated bacteria were exposed to UVA light for 30 min (Figures 4d and 5d). The structural and morphological changes of the biofilms were observed by taking SEM images.[45] Figure 4e shows typical characteristics of *E. coli* biofilms, and Figure 4f shows samples treated with PSO−ethosomes followed by UVA irradiation, which contain significantly fewer bacteria and have lost the typical arrangement of a biofilm. A similar effect was observed for *S. aureus* biofilms (Figure 5e,f). The antibiofilm activity of PSO−ethosomes suggests that ethanol entrapped in the ethosome acts as a permeation enhancer due to a synergistic mechanism between ethanol-containing vesicles and the bacterial membrane.[46] Our findings suggest that PSO−ethosomes possess increased permeability and an improved release rate because ethanol has a fluidizing effect on phospholipid bilayers, which allow the ethosomes to more easily penetrate through the bacterial cell wall. Therefore, drug-containing ethosomes exhibit more efficient photochemical activity for the inhibition of bacterial biofilm growth. These studies on the photoinduced dynamics of PSO−ethosomes as an efficient drug delivery vehicle will be helpful in the design of future photodynamic agents.

CONCLUSIONS

In the present study, we evaluated the photoinduced dynamics of PSO, a photobiologically important drug, upon encapsulation in ethosomes. We characterized PSO−ethosomes both structurally and spectroscopically. In addition, we performed solvent relaxation studies in confined environments using DCM as a model fluorophore. Picosecond-resolved FRET revealed the binding of drug molecules in the vesicles. It is inferred that there is a nonradiative energy transfer from PSO to CV upon excitation with UVA light. Furthermore, the increase in cytotoxicity of PSO-loaded ethosomes is found to be responsible for their improved antimicrobial activity. The antibiofilm activity of PSO-loaded ethosomes against both Gram-negative and -positive bacteria is also confirmed. Hence, these studies will pave the way in the design of novel, high-potential therapeutic drugs with improved pharmacological efficacy to treat multi-drug-resistant bacteria-induced diseases.

EXPERIMENTAL SECTION

Materials. Analytical grade PSO, L-α-phosphatidylcholin from soybean (PC), and CV were purchased from Sigma-Aldrich, India. DCM was purchased from Exciton, USA. All reagents were used without further purification. Ethanol (Merck, India) and water (Milli-Q, USA) were used as solvents.

Synthesis of PSO- and DCM-Containing Ethosomes. PSO and DCM were completely soluble in ethanol, and their concentrations were estimated from known extinction coefficients. Five milligrams of PC was dissolved in 40 μL of an ethanolic solution of PSO or DCM and injected rapidly in warm water (~40 °C) followed by vigorous stirring. The solution was filtered through a 0.22 μm syringe filter (Millex-GP, USA).

Characterization Methods. Absorption spectra were taken on a Shimadzu UV-2600 spectrophotometer using a quartz cell of 1 cm path length. Steady state fluorescence measurements were performed using a Jobin Yvon Fluorolog, keeping the excitation and emission bandwidth slits at 2 nm. The steady state emission of all samples was taken upon excitation at 375 nm. The size distribution and hydrodynamic diameter (d_H) of the ethosomes were measured from DLS experiments, performed on a Nano S Malvern instrument (4 mW, He−Ne laser, λ= 632.8 nm). Details of the experimental techniques are described in our previous papers.[47]

Picosecond-resolved spectroscopic studies were done using a commercial time correlated single photon counting (TCSPC) setup from Edinburgh Instruments (instrument response function (IRF) = 80 ps) using excitation at 375 nm. Fluorescence photons from the sample were detected by a microchannel plate photomultiplier tube (MCP-PMT, Hammamatsu) after dispersion through a grating monochromator. For all decays, the emission polarizer was set at 54.7° (magic angle) with respect to the polarization axis of the excitation beam. The observed fluorescence transients were fitted using a nonlinear least-squares fitting procedure. More details can be found elsewhere.[25,48] To estimate the FRET efficiency and distance between donor PSO/DCM and acceptor CV, we followed the traditional methodology described in previous work.[49]

To construct TRES, we followed techniques reported from our laboratory.[50] TRES were constructed using transients detected across the emission spectrum, starting from 500 to 650 nm at an interval of 5 nm. The time-dependent fluorescence Stokes shifts, as estimated from TRES, were used to construct the normalized spectral shift correlation function or the solvent correlation function $C(t)$ defined as

$$C(t) = \nu(t) - \nu(\infty)/\nu(0) - \nu(\infty) \quad (1)$$

where $\nu(0)$, $\nu(t)$, and $\nu(\infty)$ are the emission maximum (in cm^{-1}) at times zero, t, and infinity, respectively.[51] The $\nu(\infty)$ values were taken to be the emission frequency beyond which an insignificant or no spectral shift was observed. The $C(t)$ function represents the temporal response of the solvent relaxation process, as occurs around the probe following its photoexcitation and the associated change in the dipole moment. Fluorescence anisotropy ($r(t)$) measurements were performed as reported in previous papers at emission maxima with the emission polarization adjusted to be parallel and perpendicular to the excitation.[50]

Bacterial Strain and Culture Conditions. The antibacterial assays were performed using the common bacterial strains *E. coli* XL1-Blue[52] and *S. aureus* MTCC 3160.[53] The *E. coli* cells were cultured at 37 °C in liquid Luria−Bertani (LB) medium. When the optical density reached ~0.6, the culture was serially diluted 1000 times with LB medium and treated with drugs. The cells were treated with ethosome and PSO−ethosome (the concentration of PSO was 85 μM) samples. The samples were then kept under UVA irradiation (λ_{max} = 390 nm) for 30 min. The photodynamic effect was studied by placing 100 μL of treated samples on LB agar plates and incubating them overnight at 37 °C. After incubation overnight, the colonies were counted. The *S. aureus* cells were cultured in a liquid grade 3 media followed by the same treatment protocol.

DOI: 10.1021/acsomega.7b00187
ACS Omega 2017, 2, 1850−1857

Development of Bacterial Biofilms. *E. coli* and *S. aureus* biofilms were cultured in their prescribed media (LB and liquid grade 3 medium, respectively) on 60 mm polycarbonate Petri dishes. Two milliliters of bacterial inoculum with an optical density of 0.8 was spread on the Petri dishes and incubated for 2 days at 37 °C. Quantification of the biofilms was done using CV [0.1% (w/v)] staining after washing the attached cells.[54] Briefly, unattached cells were aspirated from the Petri dishes, which were subsequently washed with 1 mL of water. CV solution (2 mL) was added to the dishes and removed after 30 min by aspiration. Petri dishes were washed with 1 mL of water, and the remaining CV was solubilized in 95% ethanol. The degree of CV staining was evaluated from the absorbance at 595 nm (A_{595}). A_{595} values are considered to be an index of bacteria adherance to the polycarbonate surface and forming a biofilm.[55] To study the morphological changes in the biofilms upon different treatment conditions, 200 μL of the respective bacterial broth was kept over coverslips for 24 h at 37 °C, followed by washing in water. The samples were fixed with 2.5% glutaraldehyde followed by successive dehydration in alcohol and air. A qualitative assessment of the appearance of the biofilms was performed by scanning electron microscopy. The coverslips were coated with gold and scanned in a field emission scanning electron microscope (Quanta FEG 250: source of electrons, FEG source; operational accelerating voltage, 200 V to 30 kV; resolution, 30 kV under low vacuum conditions: 3.0 nm; detectors, large field secondary electron detector for low vacuum operation).

AUTHOR INFORMATION

Corresponding Author

*E-mail: skpal@bose.res.in. Telephone: +91 033 2335 5706-08. Fax: +91 033 2335 3477.

ORCID

Samir Kumar Pal: 0000-0001-6943-5828

Author Contributions

†D.B. and S.D. contributed equally to this work.

Notes

The authors declare no competing financial interest.

ACKNOWLEDGMENTS

D.B. thanks the Department of Science and Technology (DST, India) for INSPIRE fellowship. We thank the Department of Biotechnology (DBT, India) (BT/PR11534/NNT/28/766/2014) and ICMR (5/3/8/247/2014ITR) for financial support.

REFERENCES

(1) Dougherty, T. J.; Gomer, C. J.; Henderson, B. W.; Jori, G.; Kessel, D.; Korbelik, M.; Moan, J.; Peng, Q. Photodynamic Therapy. *J. Natl. Cancer Inst* **1998**, *90*, 889−905.

(2) Hamblin, M. R.; Hasan, T. Photodynamic therapy: a new antimicrobial approach to infectious disease? *Photochem. Photobiol. Sci.* **2004**, *3*, 436−450.

(3) Mehraban, N.; Freeman, H. S. Developments in PDT sensitizers for increased selectivity and singlet oxygen production. *Materials* **2015**, *8*, 4421−4456.

(4) Dolmans, D. E. J. G. J.; Fukumura, D.; Jain, R. K. Photodynamic therapy for cancer. *Nat. Rev. Cancer* **2003**, *3*, 380−387.

(5) Castano, A. P.; Demidova, T. N.; Hamblin, M. R. Mechanisms in photodynamic therapy: part one—photosensitizers, photochemistry and cellular localization. *Photodiagn. Photodyn. Ther.* **2004**, *1*, 279−293.

(6) Chimichi, S.; Boccalini, M.; Cosimelli, B.; Viola, G.; Vedaldi, D.; Dall'Acqua, F. A convenient synthesis of psoralens. *Tetrahedron* **2002**, *58*, 4859−4863.

(7) Cimino, G. D.; Shi, Y. B.; Hearst, J. E. Wavelength dependence for the photoreversal of a psoralen-DNA crosslink. *Biochemistry* **1986**, *25*, 3013−3020.

(8) Laskin, J. D.; Lee, E.; Yurkow, E. J.; Laskin, D. L.; Gallo, M. A. A possible mechanism of psoralen phototoxicity not involving direct interaction with DNA. *Proc. Natl. Acad. Sci. U. S. A.* **1985**, *82*, 6158−6162.

(9) Dall'Acqua, F.; Marciani, S.; Rodighiero, G. Inter-strand cross-linkages occurring in the photoreaction between psoralen and DNA. *FEBS Lett.* **1970**, *9*, 121−123.

(10) Hearst, J. E. Psoralen photochemistry and nucleic acid structure. *J. Invest. Dermatol.* **1981**, *77*, 39−44.

(11) Gottlieb, A. B. Psoriasis: emerging therapeutic strategies. *Nat. Rev. Drug Discovery* **2005**, *4*, 19−34.

(12) Briffa, D. V.; Warin, A. Photochemotherapy in psoriasis: a review. *J. R. Soc. Med.* **1979**, *72*, 440−446.

(13) Hannun, Y. A.; Obeid, L. M. Principles of bioactive lipid signalling: lessons from sphingolipids. *Nat. Rev. Mol. Cell Biol.* **2008**, *9*, 139−150.

(14) Kammerau, B.; Klebe, U.; Zesch, A.; Schaefer, H. Penetration, permeation, and resorption of 8-methoxypsoralen. *Arch. Dermatol. Res.* **1976**, *255*, 31−42.

(15) dos Santos, D. J.; Eriksson, L. A. Permeability of psoralen derivatives in lipid membranes. *Biophys. J.* **2006**, *91*, 2464−2474.

(16) Allen, T. M.; Cullis, P. R. Drug Delivery Systems: Entering the Mainstream. *Science* **2004**, *303*, 1818−1822.

(17) Roy, A.; Kundu, N.; Banik, D.; Sarkar, N. Comparative Fluorescence Resonance Energy-Transfer Study in Pluronic Triblock Copolymer Micelle and Niosome Composed of Biological Component Cholesterol: An Investigation of Effect of Cholesterol and Sucrose on the FRET Parameters. *J. Phys. Chem. B* **2016**, *120*, 131−142.

(18) Fielding, R. M. Liposomal Drug Delivery. *Clin. Pharmacokinet.* **1991**, *21*, 155−164.

(19) Touitou, E.; Dayan, N.; Bergelson, L.; Godin, B.; Eliaz, M. Ethosomes — novel vesicular carriers for enhanced delivery: characterization and skin penetration properties. *J. Controlled Release* **2000**, *65*, 403−418.

(20) Dayan, N.; Touitou, E. Carriers for skin delivery of trihexyphenidyl HCl: ethosomes vs. liposomes. *Biomaterials* **2000**, *21*, 1879−1885.

(21) Parashar, T.; Sachan, R.; Singh, V.; Singh, G.; Tyagi, S.; Patel, C.; Gupta, A. Ethosomes: A recent vesicle of transdermal drug delivery system. *Int. J. Res. Dev. Pharm. Life Sci.* **2013**, *2*, 285−292.

(22) Ascenso, A.; Raposo, S.; Batista, C.; Cardoso, P.; Mendes, T.; Praça, F. G.; Bentley, M. V. L. B.; Simões, S. Development, characterization, and skin delivery studies of related ultradeformable vesicles: transfersomes, ethosomes, and transethosomes. *Int. J. Nanomed.* **2015**, *10*, 5837.

(23) Zhang, Y.-T.; Shen, L.-N.; Wu, Z.-H.; Zhao, J.-H.; Feng, N.-P. Comparison of ethosomes and liposomes for skin delivery of psoralen for psoriasis therapy. *Int. J. Pharm.* **2014**, *471*, 449−452.

(24) Dubey, V.; Mishra, D.; Nahar, M.; Jain, V.; Jain, N. K. Enhanced transdermal delivery of an anti-HIV agent via ethanolic liposomes. *Nanomedicine* **2010**, *6*, 590−596.

(25) Sardar, S.; Chaudhuri, S.; Kar, P.; Sarkar, S.; Lemmens, P.; Pal, S. K. Direct observation of key photoinduced dynamics in a potential nano-delivery vehicle of cancer drugs. *Phys. Chem. Chem. Phys.* **2015**, *17*, 166−177.

(26) Chaudhuri, S.; Sardar, S.; Bagchi, D.; Dutta, S.; Debnath, S.; Saha, P.; Lemmens, P.; Pal, S. K. Photoinduced Dynamics and Toxicity of a Cancer Drug in Proximity of Inorganic Nanoparticles under Visible Light. *ChemPhysChem* **2016**, *17*, 270−277.

(27) Bagchi, D.; Chaudhuri, S.; Sardar, S.; Choudhury, S.; Polley, N.; Lemmens, P.; Pal, S. K. Modulation of stability and functionality of a

DOI: 10.1021/acsomega.7b00187
ACS Omega 2017, 2, 1850−1857

phyto-antioxidant by weakly interacting metal ions: curcumin in aqueous solution. *RSC Adv.* **2015**, *5*, 102516−102524.
(28) Zhang, Y.-T.; Shen, L.-N.; Zhao, J.-H.; Feng, N.-P. Evaluation of psoralen ethosomes for topical delivery in rats by using in vivo microdialysis. *Int. J. Nanomed.* **2014**, *9*, 669.
(29) Meyer, M.; Mialocq, J. Ground state and singlet excited state of laser dye DCM: Dipole moments and solvent induced spectral shifts. *Opt. Commun.* **1987**, *64*, 264−268.
(30) Pal, S. K.; Sukul, D.; Mandal, D.; Sen, S.; Bhattacharyya, K. Solvation dynamics of DCM in micelles. *Chem. Phys. Lett.* **2000**, *327*, 91−96.
(31) Banerjee, S.; Goswami, N.; Pal, S. K. A Potential Carcinogenic Pyrene Derivative under Förster Resonance Energy Transfer to Various Energy Acceptors in Nanoscopic Environments. *ChemPhysChem* **2013**, *14*, 3581−3593.
(32) Wang, L.-S.; Gupta, A.; Rotello, V. M. Nanomaterials for the Treatment of Bacterial Biofilms. *ACS Infect. Dis.* **2016**, *2*, 3−4.
(33) Davies, D. G.; Parsek, M. R.; Pearson, J. P.; Iglewski, B. H.; Costerton, J. t.; Greenberg, E. The involvement of cell-to-cell signals in the development of a bacterial biofilm. *Science* **1998**, *280*, 295−298.
(34) Ishiyama, M.; Tominaga, H.; Shiga, M.; Sasamoto, K.; Ohkura, Y.; Ueno, K. A combined assay of cell viability and in vitro cytotoxicity with a highly water-soluble tetrazolium salt, neutral red and crystal violet. *Biol. Pharm. Bull.* **1996**, *19*, 1518−1520.
(35) Mantulin, W. W.; Song, P.-S. Excited states of skin-sensitizing coumarins and psoralens. Spectroscopic studies. *J. Am. Chem. Soc.* **1973**, *95*, 5122−5129.
(36) Lai, T. I.; Lim, B. T.; Lim, E. Photophysical properties of biologically important molecules related to proximity effects: psoralens. *J. Am. Chem. Soc.* **1982**, *104*, 7631−7635.
(37) Pal, S. K.; Mandal, D.; Sukul, D.; Bhattacharyya, K. Solvation dynamics of 4-(dicyanomethylene)-2-methyl-6-(p-dimethylaminostyryl)-4H-pyran (DCM) in a microemulsion. *Chem. Phys. Lett.* **1999**, *312*, 178−184.
(38) Sen, P.; Mukherjee, S.; Patra, A.; Bhattacharyya, K. Solvation dynamics of DCM in a DPPC vesicle entrapped in a sodium silicate derived sol-gel matrix. *J. Phys. Chem. B* **2005**, *109*, 3319−3323.
(39) Datta, A.; Pal, S. K.; Mandal, D.; Bhattacharyya, K. Solvation dynamics of coumarin 480 in vesicles. *J. Phys. Chem. B* **1998**, *102*, 6114−6117.
(40) Fee, R.; Maroncelli, M. Estimating the time-zero spectrum in time-resolved emmsion measurements of solvation dynamics. *Chem. Phys.* **1994**, *183*, 235−247.
(41) Khara, D. C.; Samanta, A. Solvation dynamics and red-edge effect of two electrically charged solutes in an imidazolium ionic liquid. *Indian J. Chem.* **2010**, *49*, 714−720.
(42) Huang, C.-H. Phosphatidylcholine vesicles. Formation and physical characteristics. *Biochemistry* **1969**, *8*, 344−352.
(43) Marano, R. J.; Wallace, H. J.; Wijeratne, D.; Fear, M. W.; San Wong, H.; O'Handley, R. Secreted biofilm factors adversely affect cellular wound healing responses in vitro. *Sci. Rep.* **2015**, *5*, 13296.
(44) Li, X.; Kong, H.; Mout, R.; Saha, K.; Moyano, D. F.; Robinson, S. M.; Rana, S.; Zhang, X.; Riley, M. A.; Rotello, V. M. Rapid identification of bacterial biofilms and biofilm wound models using a multichannel nanosensor. *ACS Nano* **2014**, *8*, 12014−12019.
(45) Granillo, A. R.; Canales, M. G. M.; Espíndola, M. E. S.; Rivera, M. A. M.; de Lucio, V. M. B.; Tovar, A. V. R. Antibiosis interaction of Staphylococccus aureus on Aspergillus fumigatus assessed in vitro by mixed biofilm formation. *BMC Microbiol.* **2015**, *15*, 33.
(46) Morones-Ramirez, J. R.; Winkler, J. A.; Spina, C. S.; Collins, J. J. Silver Enhances Antibiotic Activity Against Gram-negative Bacteria. *Sci. Transl. Med.* **2013**, *5*, 190ra181.
(47) Rakshit, S.; Goswami, N.; Pal, S. K. Slow Solvent Relaxation Dynamics of Nanometer Sized Reverse Micellar Systems Through Tryptophan Metabolite, Kynurenine. *Photochem. Photobiol.* **2012**, *88*, 38−45.
(48) Bagchi, D.; Ghosh, A.; Singh, P.; Dutta, S.; Polley, N.; Althagafi, I. I.; Jassas, R. S.; Ahmed, S. A.; Pal, S. K. Allosteric Inhibitory Molecular Recognition of a Photochromic Dye by a Digestive Enzyme: Dihydroindolizine makes α-chymotrypsin Photo-responsive. *Sci. Rep.* **2016**, *6*, 34399.
(49) Singh, P.; Choudhury, S.; Chandra, G. K.; Lemmens, P.; Pal, S. K. Molecular recognition of genomic DNA in a condensate with a model surfactant for potential gene-delivery applications. *J. Photochem. Photobiol., B* **2016**, *157*, 105−112.
(50) Lakowicz, J. R. *Principles of Fluorescence Spectroscopy*; Springer Science & Business Media, 2013.
(51) Horng, M.; Gardecki, J.; Papazyan, A.; Maroncelli, M. Subpicosecond measurements of polar solvation dynamics: coumarin 153 revisited. *J. Phys. Chem.* **1995**, *99*, 17311−17337.
(52) Leung, Y. H.; Xu, X.; Ma, A. P.; Liu, F.; Ng, A. M.; Shen, Z.; Gethings, L. A.; Guo, M. Y.; Djurišić, A. B.; Lee, P. K.; et al. Toxicity of ZnO and TiO2 to Escherichia coli cells. *Sci. Rep.* **2016**, *6*, 35243.
(53) Applerot, G.; Lipovsky, A.; Dror, R.; Perkas, N.; Nitzan, Y.; Lubart, R.; Gedanken, A. Enhanced antibacterial activity of nanocrystalline ZnO due to increased ROS-mediated cell injury. *Adv. Funct. Mater.* **2009**, *19*, 842−852.
(54) Graziano, T. S.; Cuzzullin, M. C.; Franco, G. C.; Schwartz-Filho, H. O.; de Andrade, E. D.; Groppo, F. C.; Cogo-Müller, K. Statins and Antimicrobial Effects: Simvastatin as a Potential Drug against Staphylococcus aureus Biofilm. *PLoS One* **2015**, *10*, e0128098.
(55) Mathur, T.; Singhal, S.; Khan, S.; Upadhyay, D.; Fatma, T.; Rattan, A. Detection of biofilm formation among the clinical isolates of staphylococci: an evaluation of three different screening methods. *Indian J. Med. Microbiol.* **2006**, *24*, 25.

DOI: 10.1021/acsomega.7b00187
ACS Omega 2017, 2, 1850−1857